



**HAL**  
open science

## Evaluation of multi-modal, multi-site neuroimaging measures in Huntington's disease: Baseline results from the PADDINGTON study

Nicola Z. Hobbs, James H. Cole, Ruth E. Farmer, Elin M. Rees, Helen E. Crawford, Ian B. Malone, Raymund A.C. Roos, Reiner Sprengelmeyer, Alexandra Durr, Bernhard Landwehrmeyer, et al.

### ► To cite this version:

Nicola Z. Hobbs, James H. Cole, Ruth E. Farmer, Elin M. Rees, Helen E. Crawford, et al.. Evaluation of multi-modal, multi-site neuroimaging measures in Huntington's disease: Baseline results from the PADDINGTON study. *Neuroimage-Clinical*, 2013, 2, pp.204-211. 10.1016/j.nicl.2012.12.001 . hal-01586924

**HAL Id: hal-01586924**

**<https://hal.sorbonne-universite.fr/hal-01586924>**

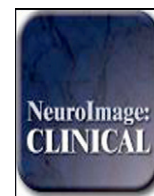
Submitted on 13 Sep 2017

**HAL** is a multi-disciplinary open access archive for the deposit and dissemination of scientific research documents, whether they are published or not. The documents may come from teaching and research institutions in France or abroad, or from public or private research centers.

L'archive ouverte pluridisciplinaire **HAL**, est destinée au dépôt et à la diffusion de documents scientifiques de niveau recherche, publiés ou non, émanant des établissements d'enseignement et de recherche français ou étrangers, des laboratoires publics ou privés.



Distributed under a Creative Commons Attribution 4.0 International License



## Evaluation of multi-modal, multi-site neuroimaging measures in Huntington's disease: Baseline results from the PADDINGTON study



Nicola Z. Hobbs<sup>a</sup>, James H. Cole<sup>a</sup>, Ruth E. Farmer<sup>b</sup>, Elin M. Rees<sup>a</sup>, Helen E. Crawford<sup>a</sup>, Ian B. Malone<sup>a</sup>, Raymund A.C. Roos<sup>c</sup>, Reiner Sprengelmeyer<sup>d</sup>, Alexandra Durr<sup>e</sup>, Bernhard Landwehrmeyer<sup>d</sup>, Rachael I. Scahill<sup>a</sup>, Sarah J. Tabrizi<sup>a</sup>, Chris Frost<sup>b,\*</sup>

<sup>a</sup> UCL Institute of Neurology, University College London, Queen Square, London WC1N 3BG, UK

<sup>b</sup> Department of Medical Statistics, London School of Hygiene and Tropical Medicine, London, UK

<sup>c</sup> Department of Neurology, Leiden University Medical Centre, Leiden, Netherlands

<sup>d</sup> Department of Neurology, Ulm University, Ulm, Germany

<sup>e</sup> Department of Genetics and Cytogenetics, and INSERM UMR S679, APHP Hôpital de la Salpêtrière, Paris, France

### ARTICLE INFO

#### Article history:

Received 18 October 2012

Received in revised form 30 November 2012

Accepted 1 December 2012

Available online 9 December 2012

#### Keywords:

Huntington's disease  
MRI  
Diffusion  
Volumetric

### ABSTRACT

**Background:** Macro- and micro-structural neuroimaging measures provide valuable information on the pathophysiology of Huntington's disease (HD) and are proposed as biomarkers. Despite theoretical advantages of microstructural measures in terms of sensitivity to pathology, there is little evidence directly comparing the two.

**Methods:** 40 controls and 61 early HD subjects underwent 3 T MRI (T1- and diffusion-weighted), as part of the PADDINGTON study. Macrostructural volumetrics were obtained for the whole brain, caudate, putamen, corpus callosum (CC) and ventricles. Microstructural diffusion metrics of fractional anisotropy (FA), mean-, radial- and axial-diffusivity (MD, RD, AD) were computed for white matter (WM), CC, caudate and putamen. Group differences were examined adjusting for age, gender and site. A formal comparison of effect sizes determined which modality and metrics provided a statistically significant advantage over others.

**Results:** Macrostructural measures showed decreased regional and global volume in HD ( $p < 0.001$ ); except the ventricles which were enlarged ( $p < 0.01$ ). In HD, FA was increased in the deep grey-matter structures ( $p < 0.001$ ), and decreased in the WM (CC,  $p = 0.035$ ; WM,  $p = 0.053$ ); diffusivity metrics (MD, RD, AD) were increased for all brain regions ( $p < 0.001$ ). The largest effect sizes were for putamen volume, caudate volume and putamen diffusivity (AD, RD and MD); each was significantly larger than those for all other metrics ( $p < 0.05$ ).

**Conclusion:** The highest performing macro- and micro-structural metrics had similar sensitivity to HD pathology quantified via effect sizes. Region-of-interest may be more important than imaging modality, with deep grey-matter regions outperforming the CC and global measures, for both volume and diffusivity. FA appears to be relatively insensitive to disease effects.

© 2013 The Authors. Published by Elsevier Inc. Open access under [CC BY-NC-SA license](https://creativecommons.org/licenses/by-nc-sa/4.0/).

### 1. Introduction

Huntington's disease (HD) is an inherited neurodegenerative disorder caused by a CAG triplet repeat expansion in the gene encoding the protein huntingtin. The disease is characterised clinically by an insidious onset usually occurring in mid-late adulthood, followed by progressive abnormalities of cognition, movement and behaviour. The classic pathological hallmark of HD is early and pronounced striatal atrophy;

however, there is now a wealth of evidence showing the neurodegenerative effects of HD to be diffuse, with involvement of the white matter (WM) and extra-striatal grey matter, even prior to symptom onset (Aylward et al., 2011; de la Monte et al., 1988; Paulsen et al., 2006; Tabrizi et al., 2009, 2011, 2012).

The application of macro- and micro-structural magnetic resonance imaging (MRI) measures to large multi-site cohorts will enable better characterisation of the nature, course and clinical relevance of the neurodegenerative process in HD. Macrostructural measures, usually derived from T1-weighted MRI, represent the gross effects of neurodegeneration, namely brain atrophy. Microstructural measures, derived from diffusion-weighted MRI, are sensitive to the diffusion of water molecules through the brain and are used to make inferences regarding the microstructural properties of the tissue. Although diffusion metrics are typically used in relation to white matter, they can also offer insights into the microstructural architecture of grey matter. Interpretation of

\* Corresponding author at: Department of Medical Statistics, London School of Hygiene and Tropical Medicine, Keppel Street, London EC1Y 7HT, UK. Tel.: +44 20 7927 2242; fax: +44 20 7637 2853.

E-mail address: [Chris.frost@lshtm.ac.uk](mailto:Chris.frost@lshtm.ac.uk) (C. Frost).

diffusion metrics is complex; however, it is generally accepted that such metrics represent a combination of neural fibre density, alignment and coherence, as well as changes to cellular membranes, axonal injury/loss and demyelination — all of which influence the diffusion of water molecules through the brain. By examining a range of diffusion metrics, we can better understand the relative contribution of these processes to HD pathophysiology. For example, fractional anisotropy (FA) relates to fibre coherence/directionality of the tissue microstructure; it is highest in highly organised white matter and is thought to decrease with loss of tissue organisation or cellular integrity. Radial- and axial-diffusivity measure the rate of diffusion perpendicular and parallel to the main direction of diffusion, respectively. There is some evidence that increases in radial diffusivity are associated with demyelination of WM tracts, whereas abnormalities in axial diffusivity may be more reflective of axonal degeneration and loss (Beaulieu, 2002), thus reflecting different elements of the neurodegenerative process.

There is increasing evidence of microstructural change in white matter such as increased diffusivity and decreased FA associated with HD (Bohanna et al., 2011; Della et al., 2010; Di Paola et al., 2012; Reading et al., 2005; Rosas et al., 2006). However, diffusion measures within grey matter have produced inconsistent results, with both increased and decreased diffusivity (Mascalchi et al., 2004; Rosas et al., 2006; Seppi et al., 2006) and differences between findings in the caudate and putamen (Douaud et al., 2009; Rosas et al., 2006). There is a need to better characterise microstructural abnormalities evident in early-manifest HD using a large cohort of patients.

Although both micro- and macro-structural neuroimaging metrics are proposed as biomarkers for HD (Dumas et al., 2011; Paulsen et al., 2008; Rosas et al., 2006; Tabrizi et al., 2011, 2012; Weaver et al., 2009), there is little evidence directly comparing the two modalities in terms of their relative sensitivities. For inherent biological reasons, it is assumed that microstructural measures may show improved sensitivity to HD-related pathology compared with macrostructural measures (i.e. we would expect disruption of cellular membranes and axonal injury to precede gross morphometric changes); however, one small study comparing striatal volume with striatal Trace values suggested the opposite (Vandenberghe et al., 2009). It is difficult to draw conclusions from this early study since numbers were small (10 HD and 12 controls), the acquisition protocol was basic (3 directions for the diffusion-weighted sequence) and there was no formal statistical comparison of modalities. Conversely, another study using a voxel-wise approach to distinguish pre-clinical HD subjects from controls, found that diffusion tensor imaging (DTI) metrics gave a better separation than those derived from T1 data (Kloppel et al., 2008). Hence there is a need to perform a robust statistical evaluation of the relative sensitivities of macro- and micro-structural neuroimaging measures in HD.

To summarize, the main aims of the current study were:

- (1) To better characterise microstructural brain abnormalities evident in early HD using a large cohort of well-characterised patients and controls, examining metrics over regions-of-interest previously implicated in HD; namely the caudate, putamen, WM, CC, whole brain and lateral ventricles;
- (2) To directly compare the sensitivities of microstructural brain measures with those of well-established macrostructural measures, via robust statistical comparison of effect sizes. Such analysis enables us to determine if any of the regions or modalities investigated has a significant advantage over the others in terms of sensitivity to HD pathology. This may be particularly relevant when selecting imaging methods and modalities for observational studies and has potential implications for the design of future clinical trials. Although future longitudinal analysis will be required, it is important to first determine the cross-sectional sensitivity of these imaging measures. To our knowledge, this is the first multi-centre study to statistically evaluate effect sizes of macro- and micro-structural imaging readouts in HD.

## 2. Materials & methods

### 2.1. Participants

Forty controls and 61 early manifest HD subjects were enrolled into the PADDINGTON study from four sites across the European Union: Leiden (Netherlands), London (UK), Paris (France) and Ulm (Germany). Early HD subjects were required to be within stage I of the disease (Shoulson and Fahn, 1979), defined by a UHDRS Total Functional Capacity (TFC)  $\geq 11$ , indicating good capacity in functional realms. Control subjects were spouses, partners or gene-negative siblings of the early HD subjects. Inclusion criteria included participants being 18–65 years of age, free from major psychiatric and concomitant neurological disorders, not currently participating in a clinical drug trial and able to tolerate and safely undergo MRI. The study was approved by the local ethical committees and written informed consent was obtained from each subject. Participants were part of Work Package 2 of the PADDINGTON study (Pharmacodynamic Approaches to Demonstration of Disease-modification in Huntington's disease by SEN0014196). Work Package 2 is an observational, imaging biomarker study with assessments at baseline, 6 months and 15 months, involving a well-characterised cohort of Stage 1 HD patients and healthy controls, who undergo 3 T MRI as well as motor, cognitive and neuropsychiatric testing. In this investigation, we focus on the baseline imaging data.

### 2.2. MRI acquisition

3 T MRI data (T1- and diffusion-weighted) were acquired based on protocols previously standardised for multi-site use (Tabrizi et al., 2009). Data were pseudoanonymised and archived on a secure web portal. Quality control was performed on all datasets by UCL Institute of Neurology, London, UK (T1-weighted) and University of Ulm, Germany (diffusion-weighted). Quality checks included the following: compliance with relevant acquisition protocols (e.g. scanner model, acquisition parameters), minimal artefacts (e.g. movement, intensity) and sufficient tissue contrast for analysis. Rescans were requested where necessary. All image processing and analysis was performed blinded to participant diagnosis.

### 2.3. MRI acquisition protocols

Using 3 T MR scanners, high-resolution three-dimensional T1-weighted structural scans and diffusion-weighted images were acquired for all participants, with clinically acceptable acquisition times (i.e. <10 min per modality). In brief, for T1-weighted scans three-dimensional magnetisation-prepared rapid gradient echo (MP-RAGE) protocols were used to acquire contiguous sagittal slices with 1 mm (London, Paris, Leiden) or 1.1 mm (Ulm) slice thickness, with no inter-slice gap, giving full brain coverage. For the diffusion-weighted scans, multiple diffusion-sensitizing gradients (42 directions in London, Paris, Leiden; 47 directions in Ulm) were applied with a diffusion weighting of  $b = 1000 \text{ s/mm}^2$ . Additional reference images with no diffusion weighting ( $b = 0 \text{ s/mm}^2$ ) were acquired (7  $b_0$  images for London, Paris; 3  $b_0$  images for Ulm, 1  $b_0$  image for Leiden). Contiguous axial slices were acquired with either 2 mm (London, Paris, Leiden) or 2.2 mm slice thickness and corresponding in-plane resolution, yielding  $2 \text{ mm}^3$  and  $2.2 \text{ mm}^3$  isotropic voxels, respectively. For full details of the acquisition parameters per site see the Supplementary material.

### 2.4. Volumetric analysis

Semi-automated volumetric measurements were performed on the T1-weighted images using MIDAS (Medical Image Display and Analysis Software) (Freeborough et al., 1997). Regions-of-interest were predefined to be the caudate, putamen, CC, lateral ventricles

and whole brain. Intracranial volume (ICV), an index of head size, was also measured on each scan using a reliable semi-automated protocol (Whitwell et al., 2001). This entailed setting a lower intensity threshold at 30% of the mean brain intensity to outline the edge of the dura, on every tenth axial slice, with the presence of cortical and cerebellar tissue defining the superior and inferior boundaries, respectively. Trilinear interpolation of areas was used to generate an estimate of ICV for each participant to enable regional volumes to be standardised for head size.

Scans were corrected for intensity inhomogeneity using N3 (Sled et al., 1998). To perform the local region-of-interest segmentations (caudate, putamen, CC and lateral ventricles), each T1-weighted scan was transformed into Montreal Neurological Institute (MNI) 305 atlas space to enable consistent application of landmark-derived cut-offs included in the segmentation protocols. A 6 degrees-of-freedom (rigid) registration was used to ensure no scaling or shearing to the images during template registration, as these effects may influence the derived volumetric measurements. Segmentation of each structure was initialised using predefined intensity constraints related to the mean brain intensity of each scan; this created an initial outline of the structure. This outline was subsequently refined by expert raters, following detailed protocols validated for use in atrophied and healthy brains.

### 2.5. Diffusion analysis

Diffusion-weighted images were pre-processed by initial rigid registration to the b0 reference image, to correct for motion and eddy current distortions, and B-vectors adjusted accordingly, after which a non-linear least-squares method was used to fit the tensor at each voxel, by incorporating the data from each gradient direction. Fractional anisotropy (FA), mean-, radial-, and axial-diffusivity (MD, AD, RD) metrics were computed over four regions-of-interest (white matter, corpus callosum, caudate and putamen), as follows: (1) regions were defined on the T1-weighted image for each individual, (2) to reduce partial volume effects in the diffusion metrics, all regions were eroded by one voxel in T1-space. This was preferred to applying a threshold (e.g. FA cut-off), to avoid circularity between region definition and outcome variable, (3) eroded regions-of-interest were transformed into 'FA space' to calculate the diffusion metrics. This transformation was achieved using NiftyReg (<http://sourceforge.net/projects/niftyreg>) as follows: the T1-weighted image was registered to the FA image using a global affine initialisation step (Ourselin et al., 2001), followed by a non-linear registration step to improve local alignment (Modat et al., 2010). This approach was adopted as the differing voxel sizes and uneven distribution of susceptibility artefacts in the two modalities meant that rigid registrations were insufficient to give anatomical correspondence, particularly for subcortical structures. FA maps were chosen as the target image, as opposed to the b0 image, as visual inspection indicated greater anatomical correspondence was achieved with FA. The transformations generated during these registrations were then applied to the eroded binary regions-of-interest using trilinear interpolation, after which the regions were finalised by thresholding at 0.5 and reconverted to binary format. All transformed T1 images and regions were visually checked to ensure accuracy of registrations between modalities. Mean diffusion metrics were calculated over these regions using the `fsstats` utility within the FSL toolbox (Smith et al., 2004).

### 2.6. Regions-of-interest (ROI)

Caudate segmentation included the head and body of the caudate, with the medial border defined by the lateral ventricle, and the lateral border defined by the internal capsule (Hobbs et al., 2009). For putamen segmentation, the anterior and lateral borders were defined by the WM of the internal and external capsules respectively, whilst voxel intensity differentiated the putamen from the globus pallidus along the medial border. Segmentation of the CC was performed in the sagittal plane

and extended four slices either side of the mid-sagittal plane for each participant (i.e. each segmentation included a total of nine slices of the image). Lateral ventricular segmentation included the lateral ventricles and temporal horn of the lateral ventricles but not the third or fourth ventricles (Scahill et al., 2003). Whole-brain segmentation was performed in native space and utilised interactive thresholding to exclude non-brain material (e.g. scalp and CSF), followed by a series of morphological operations (erosions and conditional dilations) to outline the brain (Freeborough et al., 1997).

To generate global WM metrics for the diffusion analysis, a WM region was generated on the T1-weighted images. Since the diffusion-weighted sequence did not include full brain coverage (for some subjects the cerebellum was only partially covered), the 'global' white-matter region included cut-offs to ensure anatomical consistency in voxels sampled between subjects and sites. In brief, the whole-brain regions (described above) were thresholded using predefined intensity thresholds to exclude grey matter and CSF voxels. An inferior cut-off excluded all voxels inferior to the orbito-frontal WM. To reduce partial volume effects, the region was eroded by one voxel in T1-space, and further optimised by masking with the caudate and putamen segmentations (described above) and an automated grey-matter mask, generated using the expectation-maximisation algorithm (Cardoso et al., 2011) in NiftySeg (<http://niftyseg.sf.net>).

To assess the reliability of the segmentations, some subjects had their scans segmented twice, at least a week apart, by two or three different raters. Caudate, whole brain, lateral ventricles, white matter, corpus callosum and total intracranial volumes were calculated each time. For each of the ROIs, inter- and intra-rater reliabilities were calculated using the variance estimates from a crossed random effects model (Bartlett and Frost, 2008). All ROIs had both inter- and intra-rater reliabilities of greater than 0.99. For putamen volume, only a single rater calculated volumes each time. The reliability for this ROI was calculated using an intraclass correlation coefficient (ICC), and was found to have a value of 0.988.

### 2.7. Quality control of processed data

Regions and registrations were subjected to visual quality control, both in T1- and FA-space, to ensure data were reliable prior to statistical analysis. As a result some data-points are missing (Table 2). The one missing value for putamen volume was due to insufficient contrast in this region. Four participants are missing data-points for all diffusion metrics; two due to severe motion artefacts and two due to poor T1-to-FA registration. A total of seven WM regional metrics are missing because three further participants had occipital regions positioned outside the field-of-view as a result of poor head positioning. Where whole datasets were rejected (e.g. due to motion artefacts), rescans were requested but were not possible in these cases due to patient burden and/or scan-time limitations at the site.

### 2.8. Statistical methods

Each outcome was separately analysed using a generalised least squares regression model. The model allowed for different residual variances for HD subjects and controls, in line with our a priori belief that variance would be higher in HD subjects. Potential confounders of age, gender and study site were controlled for in all models. Where model checking suggested non-normality, the 95% confidence intervals (CIs) for the group differences in outcome were estimated using Bias Corrected and accelerated (BCa) bootstrapping with 2000 replications (Efron and Tibshirani, 1993). Volumes of the whole brain, caudate, putamen and corpus callosum were expressed as a percentage of intracranial volume, to standardise for differences between individuals in head-size. All other metrics were analysed as absolute values. Effect sizes for the difference in cross-sectional outcome were calculated as the estimated absolute adjusted difference in the mean of the metric between HD

subjects and controls, divided by the estimated residual standard deviation of the HD subjects. 95% CIs for the effect size were calculated using BCa bootstrapping with 2000 replications. Differences in effect sizes were calculated for each pair of outcomes. CIs for differences between each pair of effect sizes were calculated using the same bootstrap technique as previously described, with 95% and 99% CIs being calculated in order to give p-value accuracy to either 0.05 or 0.01. Whether or not to make adjustments when carrying out multiple statistical comparisons is a controversial subject (Rothman, 1990). When each statistical comparison being made is of independent scientific interest, as we believe is the case when comparing effect sizes here, there is a good argument for not making any adjustment to p-values for the fact that multiple comparisons have been made and so this is the policy we have adopted here. Throughout, a cut-off of  $p = 0.05$  was used to establish formal statistical significance, with the actual p-values also considered in the interpretation of results. All analysis was performed in STATA v12.

### 3. Results

#### 3.1. Group demographics

Forty controls and 61 early HD subjects were scanned in total. Group demographics are displayed in Table 1. Age and gender were well-balanced between groups, by design (Table 1). For the controls, each of the four study sites contributed exactly 25% of the sample. For the HD subjects, contribution from each site ranged between 21% and 28%. 5/61 HD subjects did not fulfil criteria for being within Shoulson and Fahn Stage 1 of the disease; four of these were Stage 2 and one was Stage 3 (see Table 1 for details). Medication usage by group is detailed in Inline Supplementary Table S1.

Inline Supplementary Table S1 can be found online at <http://dx.doi.org/10.1016/j.nicl.2012.12.001>.

#### 3.2. Group differences

There was no evidence of a difference in intracranial volume between controls and HD subjects,  $p = 0.54$ .

Nineteen of the 21 imaging outcomes showed highly significant differences between HD and controls at baseline ( $p < 0.01$ , Table 2).

**Table 1**  
Characteristics of the PADDINGTON Work Package 2 cohort at baseline.

| Characteristic                                       | Controls (N = 40) |           | HD Stage I (N = 61) |             |
|--|-------------------|-----------|---------------------|-------------|
| Age (years) (mean (SD); range)                       | 51.4 (8.4)        | 29.0–66.6 | 48.7 (10.8)         | 23.5–67.3   |
| Gender   |                   |           |                     |             |
| Female N (%)   | 23                | (57.5%)   | 37                  | (60.7%)     |
| Male N (%)   | 17                | (42.5%)   | 24                  | (39.3%)     |
| Centre   |                   |           |                     |             |
| Leiden N (%)   | 10                | (25%)     | 17                  | (27.9%)     |
| London N (%)   | 10                | (25%)     | 16                  | (26.2%)     |
| Paris N (%)  | 10                | (25%)     | 13                  | (21.3%)     |
| Ulm N (%)  | 10                | (25%)     | 15                  | (24.6%)     |
| Total motor score (mean (SD); range)                 | 1.4 (1.9)         | 0–7       | 20.1 (10.7)         | 6–58        |
| Total functional capacity (mean (SD); range)         | 12.98 (0.16)      | 12–13     | 11.74 (1.45)        | 5–13        |
| CAG (mean (SD); range)                               |                   |           | 43.8 (3.2)          | 39–54       |
| Disease burden score <sup>a</sup> (mean (SD); range) |                   |           | 376.5 (85.2)        | 226.4–559.2 |
| Total functional capacity breakdown N (%)            |                   |           |                     |             |
| TFC 11–13 (HD Stage 1)                               |                   |           | 56                  | (91.8%)     |
| TFC 7–10 (HD Stage 2)                                |                   |           | 4 <sup>b</sup>      | (6.6%)      |
| TFC 3–6 (HD Stage 3)                                 |                   |           | 1 <sup>c</sup>      | (1.6%)      |

<sup>a</sup> Penney et al. (1997). Disease-burden formula:  $\text{age} \times (\text{CAG} - 35.5)$ .

<sup>b</sup> 3 participants from the London site, 1 from Paris.

<sup>c</sup> 1 participant from the Paris site.

Differences for the remaining two outcomes, WM and CC FA, were borderline statistically significant ( $p = 0.053$  and  $0.035$ , respectively).

The macrostructural outcomes provided strong evidence of decreased regional and global volume in HD subjects compared with controls ( $p < 0.001$ ), with exception of the lateral ventricles which were significantly enlarged, as expected ( $p < 0.01$ , bootstrapped, Table 2).

In the HD group, FA was increased in the grey-matter structures examined (caudate and putamen,  $p < 0.001$ ) and decreased in the white-matter structures examined (CC,  $p = 0.035$ , and global WM,  $p = 0.053$ ), compared with controls. For all other diffusion metrics (mean-, radial- and axial-diffusivity), increased levels were observed in HD subjects compared with controls, for all brain regions investigated ( $p < 0.001$ , Table 2).

#### 3.3. Comparison of effect sizes

Fig. 1A presents the estimated effect sizes and 95% CI for each of the 21 outcomes, grouped by imaging metric and modality (for values, see Inline Supplementary Table S2). Fig. 1B displays the statistical results of comparisons between effect sizes for each pair of imaging metrics.

Inline Supplementary Table S2 can be found online at <http://dx.doi.org/10.1016/j.nicl.2012.12.001>.

The two largest effect sizes were observed for the macrostructural metrics of putamen volume and caudate volume, with estimates of 2.41 (95% CIs: 1.75, 2.94) and 2.35 (95% CI: 1.58, 2.96), respectively. These effect sizes were significantly larger than for all of the other metrics ( $p < 0.05$ ), with exception of axial-, radial- and mean-diffusivity in the putamen (Fig. 1B). The other macrostructural outcomes of whole-brain, lateral ventricular and CC volume showed comparatively smaller effect sizes of around one or less (Fig. 1A).

Structure-specific diffusivity effect sizes were broadly similar irrespective of measurement (i.e. radial, axial or mean). Diffusivity effect sizes were largest for the putamen, followed by the caudate, with comparison between effect sizes for these two structures not statistically significant for each of the three diffusivity metrics. The putamen diffusivity effect sizes were significantly greater than the WM and CC diffusivity metrics (Fig. 1B).

The FA effect sizes were smaller in magnitude than those for both the volume and diffusivity metrics for the corresponding structure, and were significantly smaller than those for all other putamen metrics, as well as caudate volume and caudate axial diffusivity ( $p < 0.01$ , Fig. 1B).

### 4. Discussion

#### 4.1. Comparative sensitivities of neuroimaging metrics and modalities

Macro- and micro-structural neuroimaging measures provide valuable information on the pathophysiology of neurodegenerative diseases such as HD, and are proposed as biomarker candidates. In this study we directly interrogated the relative sensitivities of both T1-volumetric and diffusion-tensor derived metrics over a range of pathologically-implicated regions-of-interest, via a statistical comparison of effect sizes. We found similar sensitivity to HD pathology between the highest performing T1-weighted metrics (putamen and caudate volume) and the highest performing diffusion metrics (putamen diffusivity – mean, radial and axial). This is perhaps surprising; neurodegeneration in HD is a slow process where neurons undergo prolonged alterations including axonal- and dendritic-remodelling prior to gross morphometric change; hence, we had hypothesized that the microstructural diffusion metrics would show significant advantages in sensitivity over the macrostructural volumetrics. However, the reliance of diffusion MRI on echo planar imaging confers on it a reduced signal-to-noise ratio and concomitant decrease in spatial resolution compared with T1-weighted imaging. These factors are likely

**Table 2**  
Baseline imaging results for each group, and between-group differences adjusted for age, gender and study site.

| Metric   | Brain region             | Controls |       |       | HD Stage 1 |       |       | Adjusted difference in means |                  |            |
|--|--------------------------|----------|-------|-------|------------|-------|-------|------------------------------|------------------|------------|
|  |                          | N        | Mean  | SD    | N          | Mean  | SD    | Estimate                     | 95% CI           | p-Value    |
| Volume   | Putamen (% TIV)          | 40       | 0.54  | 0.06  | 60         | 0.35  | 0.08  | -0.195                       | (-0.224, -0.166) | <0.001     |
|  | Caudate (% TIV)          | 40       | 0.54  | 0.05  | 61         | 0.36  | 0.07  | -0.172                       | (-0.195, -0.148) | <0.001     |
|  | Whole brain (% TIV)      | 40       | 80.03 | 3.38  | 61         | 75.74 | 4.99  | -4.721                       | (-6.100, -3.342) | <0.001     |
|  | Lateral ventricular (ml) | 40       | 20.32 | 12.71 | 61         | 28.46 | 14.12 | 9.972                        | (5.014, 14.095)  | <0.01 (BS) |
|  | CC (% TIV)               | 40       | 0.37  | 0.05  | 61         | 0.32  | 0.06  | -0.054                       | (-0.076, -0.032) | <0.001     |
| Fractional anisotropy                                      | Putamen                  | 39       | 0.24  | 0.03  | 58         | 0.25  | 0.04  | 0.020                        | (0.011, 0.030)   | <0.001     |
|  | Caudate                  | 39       | 0.22  | 0.02  | 58         | 0.24  | 0.03  | 0.022                        | (0.014, 0.030)   | <0.001     |
|  | WM                       | 35       | 0.47  | 0.02  | 58         | 0.46  | 0.02  | -0.008                       | (-0.016, 0.000)  | 0.053      |
|  | CC                       | 39       | 0.66  | 0.04  | 58         | 0.64  | 0.05  | -0.015                       | (-0.029, -0.001) | 0.035      |
| Mean diffusivity (mm <sup>2</sup> /s) × 10 <sup>-3</sup>   | Putamen                  | 39       | 0.72  | 0.04  | 58         | 0.85  | 0.08  | 0.134                        | (0.113, 0.155)   | <0.001     |
|  | Caudate                  | 39       | 0.94  | 0.09  | 58         | 1.07  | 0.14  | 0.132                        | (0.102, 0.161)   | <0.001     |
|  | WM                       | 35       | 0.74  | 0.02  | 58         | 0.76  | 0.02  | 0.020                        | (0.011, 0.029)   | <0.001     |
|  | CC                       | 39       | 0.90  | 0.06  | 58         | 0.94  | 0.08  | 0.049                        | (0.029, 0.069)   | <0.001     |
| Radial diffusivity (mm <sup>2</sup> /s) × 10 <sup>-3</sup> | Putamen                  | 39       | 0.64  | 0.04  | 58         | 0.75  | 0.07  | 0.111                        | (0.092, 0.131)   | <0.001     |
|  | Caudate                  | 39       | 0.85  | 0.08  | 58         | 0.95  | 0.13  | 0.112                        | (0.084, 0.139)   | <0.001     |
|  | WM                       | 35       | 0.54  | 0.03  | 58         | 0.56  | 0.03  | 0.020                        | (0.010, 0.030)   | <0.001     |
|  | CC                       | 39       | 0.51  | 0.07  | 58         | 0.55  | 0.08  | 0.040                        | (0.017, 0.063)   | 0.001      |
| Axial diffusivity (mm <sup>2</sup> /s) × 10 <sup>-3</sup>  | Putamen                  | 39       | 0.90  | 0.04  | 58         | 1.07  | 0.11  | 0.179                        | (0.152, 0.205)   | <0.001     |
|  | Caudate                  | 39       | 1.13  | 0.10  | 58         | 1.29  | 0.16  | 0.172                        | (0.139, 0.205)   | <0.001     |
|  | WM                       | 35       | 1.14  | 0.02  | 58         | 1.16  | 0.02  | 0.021                        | (0.011, 0.030)   | <0.001     |
|  | CC                       | 39       | 1.67  | 0.09  | 58         | 1.73  | 0.09  | 0.066                        | (0.038, 0.094)   | <0.001     |

(BS) 95% CI obtained using bootstrapping (BCa interval) due to non-normality of residuals from primary model. p-Value accurate to <0.05 or <0.01. WM=white matter; CC=corpus callosum.

to mitigate the advantages that the technique offers in detecting abnormalities.

Our findings show that the region-of-interest examined may be more important than the imaging modality applied, with the subcortical grey-matter regions outperforming the global measures and corpus callosum for both macro- and micro-structural metrics. The exceptions were the FA results for the caudate and putamen, which ranked much lower in the effect-size table; 14th and 17th out of the 21 imaging outcomes, respectively. At least cross-sectionally, FA measures appear to be relatively insensitive to HD pathology in early manifest disease.

In the context of biomarker candidates, when deciding between metrics which are not significantly different, other factors may come into play, such as time and ease of acquisition, image analysis costs, whether the metrics provide independent information on neurodegeneration and whether they show significant alterations over time. For example, in the current cross-sectional study, caudate and putamen metrics performed very similarly in terms of effect size, which is not surprising since we would expect these structures to degenerate in parallel; hence there may be limited advantages in including measures from both regions in a study or trial. Conversely, although the CC metrics produced smaller effect sizes, the CC is not part of the basal ganglia-thalamocortical-pathway; hence, these metrics may provide unique information on neurodegeneration, independent of grey-matter degeneration. However, effect sizes for the diffusion metrics were consistently smaller than for the corresponding volumetrics (although not always significantly so); hence, this study suggests that there may be little gain in generating both T1-volumetric and diffusion-tensor metrics, in terms of cross-sectional detection of pathology in early HD patients.

#### 4.2. Characterisation of micro- and macro-structural abnormalities in early HD

This study also enabled us to better characterise the macro- and micro-structural abnormalities evident in early manifest HD on the same cohort of patients; this is the largest study cohort for DTI metrics in HD to date. We observed reduced FA, thought to reflect alterations in fibre coherence and directionality, in both the CC (Bohanna et al., 2011; Della et al., 2010; Di Paola et al., 2012; Rosas et al., 2006, 2010) and the global WM metric, concurring with findings across widespread WM regions in HD patients (Della et al., 2010; Delmaire et al., in press; Rosas et al., 2006). It has been suggested that such abnormalities

could be attributed to damaged oligodendrocytes and axonal membranes, disrupted axonal transport due to the presence of mutant huntingtin, and early increases in reactive microglia (see Bohanna et al., 2008 for discussion).

We also observed an increase of FA in the deep grey-matter structures examined. This is in accordance with most previous studies (Delmaire et al., in press; Douaud et al., 2009; Sanchez-Castaneda et al., in press; Sritharan et al., 2010), although two studies have found increased FA in the putamen but surprisingly, not the caudate (Bohanna et al., 2011; Rosas et al., 2006). Whilst FA alterations in grey-matter structures are more complicated to interpret, the observed group differences may represent selective neurodegeneration, i.e. a preferential loss of connections along specific directions radiating from the subcortical grey-matter nuclei, coupled with relative sparing of other directions; when combined these factors would make the tissue appear less isotropic. Supportive of this hypothesis is evidence from a DTI study examining the dispersion of the fibre orientations in the subcortical grey-matter structures in manifest HD, which found that the striatal-pallidal projections appeared to be the most affected (Douaud et al., 2009). The specific histological correlates of such abnormalities in grey-matter FA require further work and verification.

We observed increased mean diffusivity in the grey- and white-matter regions in the early HD group, in line with previous research (Douaud et al., 2009; Mascalchi et al., 2004; Rosas et al., 2006; Sanchez-Castaneda et al., in press; Seppi et al., 2006). To further investigate these abnormalities, we examined both radial and axial diffusivity. Radial diffusivity measures the perpendicular motion of water molecules in the fibres and is thought to be sensitive to abnormalities in the myelin sheath (Song et al., 2002). Axial diffusivity measures the motion of water molecules parallel to the fibres and abnormalities are thought to be reflective of axonal injury or degeneration (Song et al., 2003). In accordance with previous findings, we observed increased radial- and axial-diffusivity in the CC (Di Paola et al., 2012; Rosas et al., 2010). We also found the same pattern of increases across global WM in early HD, which, to our knowledge, has not been demonstrated previously. Taken together, these findings suggest that both myelin breakdown and axonal damage play an important role in the pathophysiology of HD by the time the disease manifests and that these changes are not restricted to the WM of the CC, but are present throughout the brain. In the current study, axial diffusivity abnormalities were slightly larger in magnitude than radial diffusivity, which may suggest

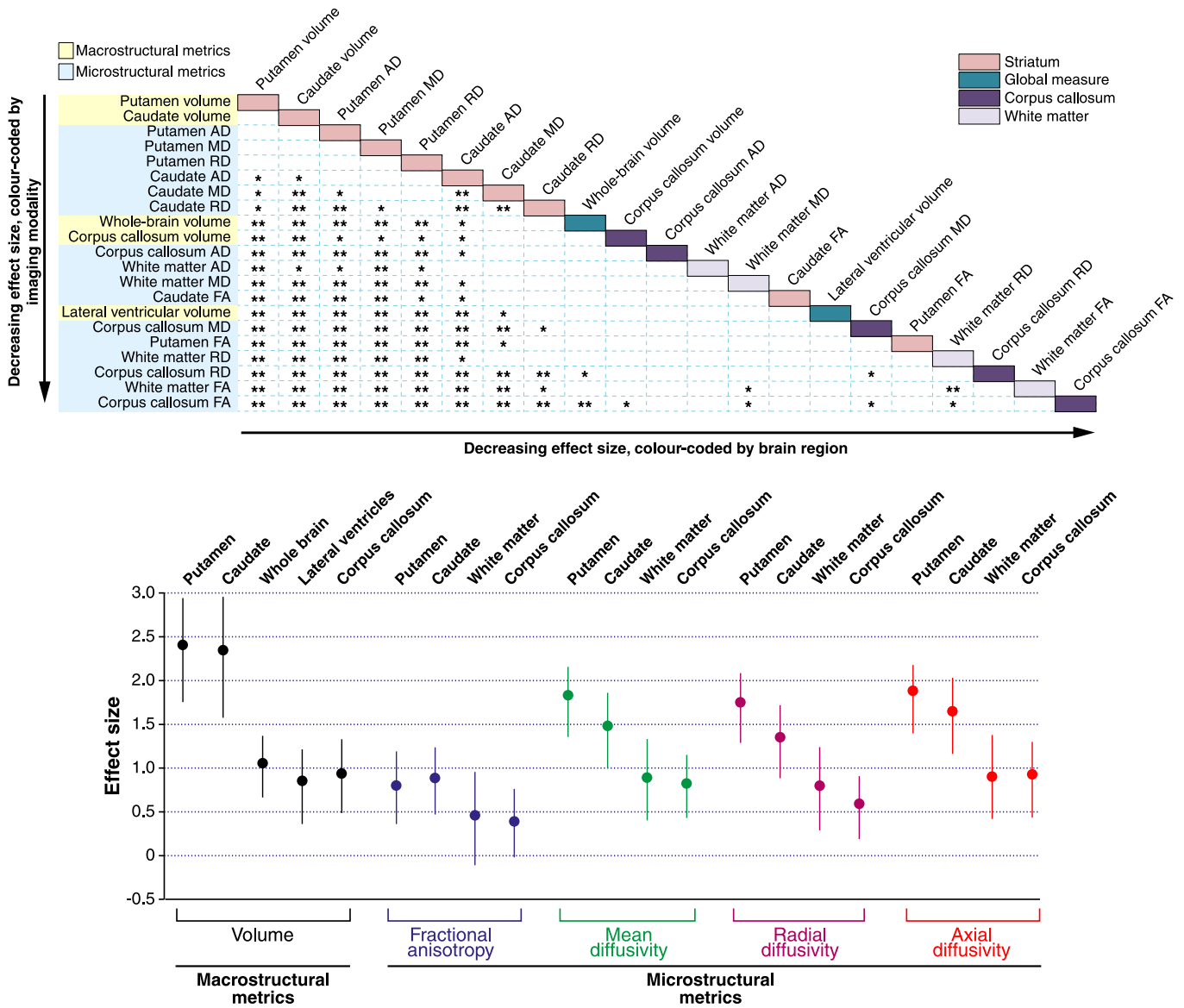


**Fig. 1.** A. Effect-size estimates (mean and 95% CIs) for each of the imaging outcomes. Data are grouped by imaging metric and modality. Effect sizes calculated as the absolute difference in the mean of the metric between groups, adjusted for age, gender and study site, divided by the estimated residual standard deviation of the HD group. B. Statistical comparison of effect sizes between imaging metrics and modalities (\*/\*\* indicates  $p < 0.05/0.01$ ). \* & \*\* denote a statistically significant difference at  $p < 0.05$  and  $p < 0.01$ , respectively, in the magnitude of the effect sizes for each pair of metrics. For example, although putamen volume had the largest effect size overall (top of the list), this was not significantly larger than that for caudate volume, putamen AD, MD or RD (absence of \* in adjacent boxes); however, it was significantly larger than that for caudate AD, MD and RD at  $p < 0.05$  (\* in each adjacent boxes), and also significantly larger than that for all other metrics at  $p < 0.01$  (\*\* in adjacent boxes). Metrics are ordered by magnitude of effect sizes and colour-coded by imaging modality (left-hand side) and brain region (right-hand side).

that axonal degeneration predominates over myelin abnormalities at this stage of the disease. Further investigations are required to verify this hypothesis. It should be noted that interpretation of the pathophysiological correlates of DTI metrics can be somewhat tenuous (Jones et al., 2012), and there may be a number of non-pathological or latent influences on changes in FA or diffusivity. Evidence that the patterns of abnormalities in diffusivity metrics described above have been shown to concur with direct histology in rodents (Song et al., 2002, 2003) does not necessarily translate to humans. Nevertheless, histological investigations of end-stage HD show substantial WM atrophy, accompanied by decreases of both myelin and axis cylinders (Tellez-Nagel et al., 1974). These post-mortem findings should give increased confidence that the diffusion metrics employed here do in fact reflect pathological processes.

Radial and axial diffusivity were also abnormal in the caudate and putamen of early HD subjects, with increases of a similar magnitude in both structures in HD patients compared with controls. To our knowledge, this is the first study to explicitly examine these diffusion metrics in early HD in the striatal structures, although a pattern of radial and axial diffusivity increasing in tandem would result in a mean diffusivity increase, which has been reported (Bohanna et al., 2011; Delmaire et al., in press; Douaud et al., 2009; Mandelli et al., 2010; Rosas et al., 2006; Sanchez-Castaneda et al., in press; Seppi et al., 2006; Sritharan et al., 2010; Vandenberghe et al., 2009). As with FA, the pathology underlying alterations in diffusivity in grey-matter is not well understood, but could reflect an increase in extra-cellular spaces due to neural tissue loss. As with the white matter, axial diffusivity changes were larger than radial changes. Speculatively, this may be

an indication that a specific neuronal population with a common orientation is atrophying, alongside the relative preservation of other cells with an oblique orientation. This hypothesis would fit with the early loss of striatal medium spiny neurons, well-characterised in neuropathological studies of HD (Kowall et al., 1987; Vonsattel et al., 1985).

As expected, our volume measures provided strong evidence of macrostructural degeneration in early HD, with highly significant differences between HD and controls for all metrics examined. Reduced regional and global volumes, coupled with increased lateral ventricular volume are in agreement with previous studies (Ciarmiello et al., 2006; Di Paola et al., 2012; Paulsen et al., 2008; Rosas et al., 2010; Tabrizi et al., 2009), as well as post mortem data of end-stage disease, which show gross atrophy of the caudate and putamen (Vonsattel et al., 1985), cortical and extra-striatal subcortical atrophy (de la Monte et al., 1988; Mann et al., 1993) accompanied by a two-fold increase in ventricular size and considerable WM reductions (de la Monte et al., 1988).

#### 4.3. Strengths

A strength of this study is that it uses a relatively large, well-characterised cohort of participants. Additionally, few studies in the literature have directly compared macro- and micro-structural imaging metrics on the same cohort, particularly not with the robust statistical approach taken in this study. Furthermore, we have analysed the diffusion data in its native space, without adjusting the voxel sizes; hence our results, particularly for the deep grey-matter structures, are unlikely to be confounded by registration error or tissue shifts as has been suggested for previous findings in the literature (see Kloppel et al., 2009 for discussion).

#### 4.4. Limitations

We acknowledge the limitations of the study. Firstly, in terms of assessing the relative advantages of biomarkers of disease progression, longitudinal assessment is essential, since cross-sectional findings cannot reliably be extrapolated to longitudinal scenarios. Hence, it will be important to repeat this analysis on longitudinal data particularly if the findings are to be used to inform clinical trial design. Also, our data were pooled from four different study sites across Europe, and despite efforts to standardised procedures, it is impossible to rule out increased noise due to site-specific factors. However the fact that our study is multi centre can also be considered a strength since it is likely that future clinical trials will involve multiple centres. Indeed, the present demonstration of significant effects using pooled imaging data should give confidence to any forthcoming multi-site studies.

#### 4.5. Conclusions

In summary, we have measured a range of macro- and micro-structural neuroimaging measures on a large cohort of early manifest HD patients and controls. All measures were sensitive to HD pathology, determined by between-group differences. However, statistical comparison of effect sizes showed no significant advantages between the highest performing macro- and micro-structural measures, with putamen volume, caudate volume and putamen diffusivity metrics proving to be the most sensitive. In future studies and trials a panel of biomarkers is likely to be required to understand the full effects of HD, and what result any intervention may have on its progression. By statistically interrogating effect sizes, we can make informed choices about which metrics are the most powerful, both cross-sectionally and longitudinally.

#### Acknowledgements

The authors would like to thank the patients and controls who took part in this study, along with all the Work Package 2 site staff at Paris,

Leiden, Ulm and London. This work has been supported by the European Union – PADDINGTON project, contract no. HEALTH-F2-2010-261358 and all authors, with the exception of RS, IM and HC, receive funding from this project. RS, IM and HC are supported by the CHDI/High Q Foundation, a not-for-profit organization dedicated to finding treatments for Huntington's disease. This work was undertaken at UCLH/UCL which received a proportion of funding from the Department of Health's NIHR Biomedical Research Centres Funding Scheme.

#### Appendix A. Supplementary data

Supplementary data to this article can be found online at <http://dx.doi.org/10.1016/j.nicl.2012.12.001>.

#### References

- Aylward, E.H., Nopoulos, P.C., Ross, C.A., Langbehn, D.R., Pierson, R.K., Mills, J.A., et al., 2011. Longitudinal change in regional brain volumes in prodromal Huntington disease. *Journal of Neurology, Neurosurgery, and Psychiatry* 82, 405–410.
- Bartlett, J.W., Frost, C., 2008. Reliability, repeatability and reproducibility: analysis of measurement errors in continuous variables. *Ultrasound in Obstetrics & Gynecology* 31, 466–475.
- Beaulieu, C., 2002. The basis of anisotropic water diffusion in the nervous system – a technical review. *NMR in Biomedicine* 15, 435–455.
- Bohanna, I., Georgiou-Karistianis, N., Hannan, A.J., Egan, G.F., 2008. Magnetic resonance imaging as an approach towards identifying neuropathological biomarkers for Huntington's disease. *Brain Research Reviews* 58, 209–225.
- Bohanna, I., Georgiou-Karistianis, N., Sriharan, A., Asadi, H., Johnston, L., Churchyard, A., et al., 2011. Diffusion tensor imaging in Huntington's disease reveals distinct patterns of white matter degeneration associated with motor and cognitive deficits. *Brain Imaging and Behavior* 5, 171–180.
- Cardoso, M.J., Clarkson, M.J., Ridgway, G.R., Modat, M., Fox, N.C., Ourselin, S., 2011. LoAd: a locally adaptive cortical segmentation algorithm. *NeuroImage* 56, 1386–1397.
- Ciarmiello, A., Cannella, M., Lastoria, S., Simonelli, M., Frati, L., Rubinsztein, D.C., et al., 2006. Brain white-matter volume loss and glucose hypometabolism precede the clinical symptoms of Huntington's disease. *Journal of Nuclear Medicine* 47, 215–222.
- de la Monte, S.M., Vonsattel, J.P., Richardson Jr., E.P., 1988. Morphometric demonstration of atrophic changes in the cerebral cortex, white matter, and neostriatum in Huntington's disease. *Journal of Neuropathology and Experimental Neurology* 47, 516–525.
- Della, N.R., Ginestroni, A., Tessa, C., Giannelli, M., Piacentini, S., Filippi, M., et al., 2010. Regional distribution and clinical correlates of white matter structural damage in Huntington disease: a tract-based spatial statistics study. *AJNR. American Journal of Neuroradiology* 31, 1675–1681.
- Delmaire, C., Dumas, E.M., Sharman, M.A., van den Bogaard, S.J., Valabregue, R., Jauffret, C., et al., in press. The structural correlates of functional deficits in early Huntington's disease. *Human Brain Mapping*. <http://dx.doi.org/10.1002/hbm.22055>.
- Di Paola, M., Luders, E., Cherubini, A., Sanchez-Castaneda, C., Thompson, P.M., Toga, A.W., et al., 2012. Multimodal MRI analysis of the corpus callosum reveals white matter differences in presymptomatic and early Huntington's disease. *Cerebral Cortex* 22, 2858–2866.
- Douaud, G., Behrens, T.E., Poupon, C., Cointepas, Y., Jbabdi, S., Gaura, V., et al., 2009. In vivo evidence for the selective subcortical degeneration in Huntington's disease. *NeuroImage* 46, 958–966.
- Dumas, E.M., van den Bogaard, S.J., Ruber, M.E., Reilman, R.R., Stout, J.C., Craufurd, D., et al., 2011. Early changes in white matter pathways of the sensorimotor cortex in premanifest Huntington's disease. *Human Brain Mapping* 33, 203–212.
- Efron, B., Tibshirani, R.J., 1993. *An Introduction to the Bootstrap*. Chapman & Hall, New York.
- Freeborough, P.A., Fox, N.C., Kitney, R.I., 1997. Interactive algorithms for the segmentation and quantitation of 3-D MRI brain scans. *Computer Methods and Programs in Biomedicine* 53, 15–25.
- Hobbs, N.Z., Henley, S.M., Wild, E.J., Leung, K.K., Frost, C., Barker, R.A., et al., 2009. Automated quantification of caudate atrophy by local registration of serial MRI: evaluation and application in Huntington's disease. *NeuroImage* 47, 1659–1665.
- Jones, D.K., Knosche, T.R., Turner, R., 2012. White matter integrity, fiber count, and other fallacies: the do's and don'ts of diffusion MRI. *NeuroImage*. <http://dx.doi.org/10.1016/j.neuroimage.2012.06.081>.
- Kloppel, S., Draganski, B., Golding, C.V., Chu, C., Nagy, Z., Cook, P.A., et al., 2008. White matter connections reflect changes in voluntary-guided saccades in pre-symptomatic Huntington's disease. *Brain* 131, 196–204.
- Kloppel, S., Henley, S.M., Hobbs, N.Z., Wolf, R.C., Kassubek, J., Tabrizi, S.J., et al., 2009. Magnetic resonance imaging of Huntington's disease: preparing for clinical trials. *Neuroscience* 164, 205–219.
- Kowall, N.W., Ferrante, R.J., Martin, J.B., 1987. Patterns of cell loss in Huntington's disease. *Trends in Neurosciences* 10, 24–29.
- Mandelli, M.L., Savoirdo, M., Minati, L., Mariotti, C., Aquino, D., Erbetta, A., et al., 2010. Decreased diffusivity in the caudate nucleus of presymptomatic Huntington disease gene carriers: which explanation? *AJNR. American Journal of Neuroradiology* 31, 706–710.

- Mann, D.M., Oliver, R., Snowden, J.S., 1993. The topographic distribution of brain atrophy in Huntington's disease and progressive supranuclear palsy. *Acta Neuropathologica* 85, 553–559.
- Mascalchi, M., Lolli, F., Della, N.R., Tessa, C., Petralli, R., Gavazzi, C., et al., 2004. Huntington disease: volumetric, diffusion-weighted, and magnetization transfer MR imaging of brain. *Radiology* 232, 867–873.
- Modat, M., Ridgway, G.R., Taylor, Z.A., Lehmann, M., Barnes, J., Hawkes, D.J., et al., 2010. Fast free-form deformation using graphics processing units. *Computer Methods and Programs in Biomedicine* 98, 278–284.
- Ourselin, S., Roche, A., Subsol, G., Pennec, X., Ayache, N., 2001. Reconstructing a 3D structure from serial histological sections. *Image and Vision Computing* 19, 25–31.
- Paulsen, J.S., Magnotta, V.A., Mikos, A.E., Paulson, H.L., Penziner, E., Andreasen, N.C., et al., 2006. Brain structure in preclinical Huntington's disease. *Biological Psychiatry* 59, 57–63.
- Paulsen, J.S., Langbehn, D.R., Stout, J.C., Aylward, E., Ross, C.A., Nance, M., et al., 2008. Detection of Huntington's disease decades before diagnosis: the Predict-HD study. *Journal of Neurology, Neurosurgery, and Psychiatry* 79, 874–880.
- Penney Jr., J.B., Vonsattel, J.P., MacDonald, M.E., Gusella, J.F., Myers, R.H., 1997. CAG repeat number governs the development rate of pathology in Huntington's disease. *Annals of Neurology* 41, 689–692.
- Reading, S.A., Yassa, M.A., Bakker, A., Dziorny, A.C., Gourley, L.M., Yallapragada, V., et al., 2005. Regional white matter change in pre-symptomatic Huntington's disease: a diffusion tensor imaging study. *Psychiatry Research* 140, 55–62.
- Rosas, H.D., Tuch, D.S., Hevelone, N.D., Zaleta, A.K., Vangel, M., Hersch, S.M., et al., 2006. Diffusion tensor imaging in presymptomatic and early Huntington's disease: selective white matter pathology and its relationship to clinical measures. *Movement Disorders* 21, 1317–1325.
- Rosas, H.D., Lee, S.Y., Bender, A.C., Zaleta, A.K., Vangel, M., Yu, P., et al., 2010. Altered white matter microstructure in the corpus callosum in Huntington's disease: implications for cortical "disconnection". *NeuroImage* 49, 2995–3004.
- Rothman, K.J., 1990. No adjustments are needed for multiple comparisons. *Epidemiology* 1, 43–46.
- Sanchez-Castaneda, C., Cherubini, A., Elifani, F., Peran, P., Orobello, S., Capelli, G., et al., in press. Seeking huntington disease biomarkers by multimodal, cross-sectional basal ganglia imaging. *Human Brain Mapping*. <http://dx.doi.org/10.1002/hbm.22019>.
- Scahill, R.I., Frost, C., Jenkins, R., Whitwell, J.L., Rossor, M.N., Fox, N.C., 2003. A longitudinal study of brain volume changes in normal aging using serial registered magnetic resonance imaging. *Archives of Neurology* 60, 989–994.
- Seppi, K., Schocke, M.F., Mair, K.J., Esterhammer, R., Weirich-Schwaiger, H., Utermann, B., et al., 2006. Diffusion-weighted imaging in Huntington's disease. *Movement Disorders* 21, 1043–1047.
- Shoulson, I., Fahn, S., 1979. Huntington disease: clinical care and evaluation. *Neurology* 29, 1–3.
- Sled, J.G., Zijdenbos, A.P., Evans, A.C., 1998. A nonparametric method for automatic correction of intensity nonuniformity in MRI data. *IEEE Transactions on Medical Imaging* 17, 87–97.
- Smith, S.M., Jenkinson, M., Woolrich, M.W., Beckmann, C.F., Behrens, T.E., Johansen-Berg, H., et al., 2004. Advances in functional and structural MR image analysis and implementation as FSL. *NeuroImage* 23 (Suppl. 1), S208–S219.
- Song, S.K., Sun, S.W., Ramsbottom, M.J., Chang, C., Russell, J., Cross, A.H., 2002. Demyelination revealed through MRI as increased radial (but unchanged axial) diffusion of water. *NeuroImage* 17, 1429–1436.
- Song, S.K., Sun, S.W., Ju, W.K., Lin, S.J., Cross, A.H., Neufeld, A.H., 2003. Diffusion tensor imaging detects and differentiates axon and myelin degeneration in mouse optic nerve after retinal ischemia. *NeuroImage* 20, 1714–1722.
- Sritharan, A., Egan, G.F., Johnston, L., Horne, M., Bradshaw, J.L., Bohanna, I., et al., 2010. A longitudinal diffusion tensor imaging study in symptomatic Huntington's disease. *Journal of Neurology, Neurosurgery, and Psychiatry* 81, 257–262.
- Tabrizi, S.J., Langbehn, D.R., Leavitt, B.R., Roos, R.A., Durr, A., Craufurd, D., et al., 2009. Biological and clinical manifestations of Huntington's disease in the longitudinal TRACK-HD study: cross-sectional analysis of baseline data. *Lancet Neurology* 8, 791–801.
- Tabrizi, S.J., Scahill, R.I., Durr, A., Roos, R.A., Leavitt, B.R., Jones, R., et al., 2011. Biological and clinical changes in premanifest and early stage Huntington's disease in the TRACK-HD study: the 12-month longitudinal analysis. *Lancet Neurology* 10, 31–42.
- Tabrizi, S.J., Reilmann, R., Roos, R.A., Durr, A., Leavitt, B., Owen, G., et al., 2012. Potential endpoints for clinical trials in premanifest and early Huntington's disease in the TRACK-HD study: analysis of 24 month observational data. *Lancet Neurology* 11, 42–53.
- Tellez-Nagel, I., Johnson, A.B., Terry, R.D., 1974. Studies on brain biopsies of patients with Huntington's chorea. *Journal of Neuropathology and Experimental Neurology* 33, 308–332.
- Vandenberghe, W., Demaerel, P., Dom, R., Maes, F., 2009. Diffusion-weighted versus volumetric imaging of the striatum in early symptomatic Huntington disease. *Journal of Neurology* 256, 109–114.
- Vonsattel, J.P., Myers, R.H., Stevens, T.J., Ferrante, R.J., Bird, E.D., Richardson Jr., E.P., 1985. Neuropathological classification of Huntington's disease. *Journal of Neuropathology and Experimental Neurology* 44, 559–577.
- Weaver, K.E., Richards, T.L., Liang, O., Laurino, M.Y., Samii, A., Aylward, E.H., 2009. Longitudinal diffusion tensor imaging in Huntington's disease. *Experimental Neurology* 216, 525–529.
- Whitwell, J.L., Crum, W.R., Watt, H.C., Fox, N.C., 2001. Normalization of cerebral volumes by use of intracranial volume: implications for longitudinal quantitative MR imaging. *AJNR. American Journal of Neuroradiology* 22, 1483–1489.